DOI https: //doi. org/10.1007/s11595-019-2184-x

Thickness Dependence of Structural and Optical Properties of Chromium Thin Films as an Infrared Reflector for Solar-thermal Conversion Applications

LI Qingyu[1], GONG Dianqing[2], CHENG Xudong[1*]

(1. State Key Laboratory of Advanced Technology for Materials Synthesis and Processing, Wuhan University of Technology, Wuhan 430070, China, 2. College of Materials Science and Engineering, Taiyuan University of Technology, Taiyuan 030024, China)

Abstract: The thermal emittance of Cr film, as an IR reflector, was investigated for the use in SSAC. The Cr thin films with different thicknesses were deposited on silicon wafers, optical quartz and stainless steel substrates by cathodic arc ion plating technology as a metallic IR reflector layer in SSAC. The thickness of Cr thin films was optimized to achieve the minimum thermal emittance. The effects of structural, microstructural, optical, surface and cross-sectional morphological properties of Cr thin films were investigated on the emittance. An optimal thickness about 450 nm of the Cr thin film for the lowest total thermal emittance of 0.05 was obtained. The experimental results suggested that the Cr metallic thin film with optimal thickness could be used as an effective infrared reflector for the development of SSAC structure.

Key words: thermal emittance; chromium thin film; solar selective absorbing coating; cathodic arc ion plating

1 Introduction

Solar energy, which is one of the most abundant sources of renewable energy, attracting attention for its easy availability, nature friendliness, and CO_2 emission free source, *etc*[1,2]. It is an important source of renewable energy and its technologies are broadly characterized as either passive solar or active solar depending on how they capture and distribute solar energy or convert it into solar power[3]. Active solar techniques include the use of photovoltaic systems, concentrated solar power and solar water heating to harness the energy[4]. Passive solar techniques include orienting a building to the sun, selecting materials with favorable thermal mass or light-dispersing properties, and designing spaces that naturally circulate air[5]. The collector, an important sub-system of the solar thermal system, is used to collect and convert the concentrated solar energy into thermal energy followed by its transfer to the fluid medium[1]. Solar selective absorbing coating (SSAC) is one of the key elements of the solar collector, which could be used as the photothermal conversion surface[6,7]. Namely, it should maximally absorb the solar radiation corresponding to blackbody radiation in the solar spectrum range (0.3-2.5 μm), and minimally emit the infrared thermal radiation in the thermal infrared range (2.5-25 μm). The typical multi-layer structure from surface to substrate is shown in Fig.1, which consists of a ceramic anti-reflection layer, a low and a high metal volume fraction cermet solar absorption layers (LMVF and HMVF), and a metal infrared (IR) reflector layer. Normally, the stainless steel, copper, and aluminum are commonly used as substrates for solar thermal applications. A cleaned substrate usually present a low thermal emittance about 0.12[8]. However, the commonly used substrates usually degrade the solar thermal performance at thermal condition, for the elements diffusion from substrate into the absorption layers.

Thus, a metal thin layer should be introduced between substrate and absorber, which not only provides low thermal emittance as an IR reflector, but also protects the solar thermal performance at thermal condition. Therefore, the reflector should exhibit high thermal tolerance as the temperature of this tandem

(Received: Jan. 12, 2019; Accepted: Apr. 23, 2019)

LI Qingyu (李擎煜): E-mail: liqingyu@whut.edu.cn

*Corresponding author: CHENG Xudong (程旭东): Prof.; Ph D; E-mail: xdcheng54@163.com

Funded by the National Natural Science Foundation of China (No. 51402208), and the Project by State Key Laboratory of Advanced Technology for Materials Synthesis and Processing (Wuhan University of Technology) (No. 2016-KF-11)

solar selective absorbing coating may increase more than 600 °C during the operational period. This infrared reflecting layer also plays an important role as a barrier layer between the substrate and absorption layers to protect the corrosion and thus providing the long-term stability to the solar selective absorbing structures. As a whole, the metal IR-reflector layer should have not only high reflectance in the IR range but also excellent thermal stability at elevated temperature.

Normally, copper (Cu)[9], silver (Ag)[10], platinum (Pt)[11], molybdenum (Mo)[12], and chromium (Cr)[13] are mostly used as reflector in the infrared region. However, the Cu, Ag, and Pt used as reflectors suffer from agglomeration after heating, which degrades the infrared reflection properties and increases the thermal emittance[1]. Additionally, the cost of these reflectors is also a major issue. As for the Mo reflector, the diffusion of carbon into the Mo layer results to higher emittance at thermal condition[14]. Thus, keeping in mind the above constrains, chromium metal is chosen as a promising candidate for IR reflector in solar absorbers for its refractory nature with high melting point (1857 ℃). SSACs with Cr metal IR reflector show a low thermal emittance, such as Cr/TiAlCrN-G/TiAlN/AlSiN/AlSiO: α=0.96, ε=0.10[15]; Cr/AlCrN/AlCrNO/AlCrO: α=0.90, ε=0.15[16]; Cr/LOCL/MOCL/HOCL: α=0.92, ε=0.21[17]. Additionally, the metal Cr is cheaper and the SSACs using the metal Cr as the IR reflector have good thermal stability above 500 ℃[15-17]. In the case of low thermal emittance of SSAC, Cr thin film is employed as IR reflector with thermal stability at thermal condition. Considering the widely usage of the Cr film in SSAC, it is valuable to study the thermal emittance and relevant optical properties of the Cr film. Nevertheless, the detailed information about the relationship between the emittance of the Cr film and thickness has not been reported so far. Meanwhile, IR reflectance of the metal films is strongly influenced by the film structure, such as crystallite size, strain and surface morphology[2]. Moreover, these properties can be affected by film thickness[18].

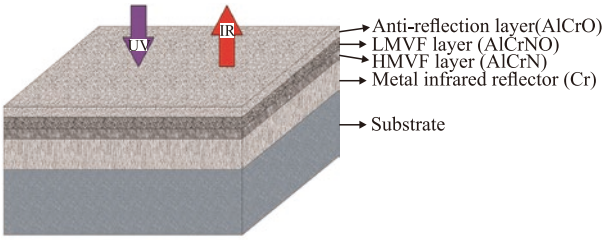

Fig.1 Schematic diagram of the typical structure of multi-layer SSAC.

Now days, numerous efforts have been made to prepare the SSAC by employing different techniques, such as chemical vapor deposition (CVD) and physical vapor deposition (PVD). As the CVD deposited coatings may cause some environmental issues and exhibit low thermal stability, the PVD deposited coatings are mostly developed for large-area deposition of SSAC[19]. Among those methods, the cathodic arc ion plating (CAIP) technology, a typical vapor deposition, has attracted wide attention due to its advantages over other thin film deposition methods, such as large adhesion force, accurate control over composition and thickness, and uniform dense surface over large areas[20-22]. Therefore, it is relevant to explore the CAIP technique for solar applications as the SSAC will inevitably demand multi-functional attributes, including high abrasion resistance that the CAIP is known to provide.

In this paper, the Cr thin films were prepared on silicon wafers, optical quartz and stainless steel substrates by CAIP as the IR reflector metallic layer in SSAC. The effect of film thickness on thermal emittance was studied and the optimal thickness,

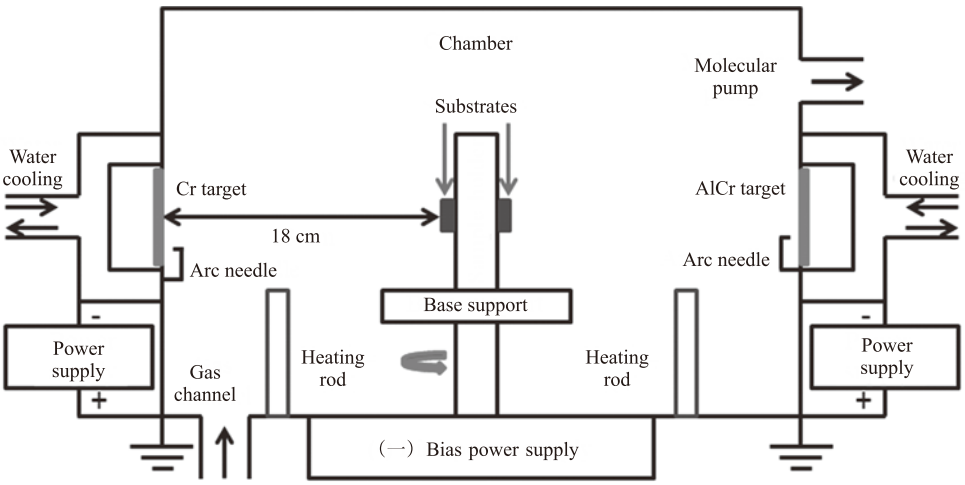

Fig.2 The schematic diagram of cathodic arc ion plating system

which made the lowest thermal emittance, was obtained. The main motivation of this paper was to optimize the thermal emittance of Cr thin films by varying the thickness, and to understand the structure-thickness correlation affecting the thermal emittance of metallic chromium thin film. Moreover, the structure, morphologies and optical constants of the Cr films were investigated in detail.

2 Experimental

2.1 Coating deposition

The Cr thin films were prepared by cathodic arc ion plating (CAIP) on (100) silicon wafers (20 cm×20 cm), JGS1 optical quartz (20 cm×20 cm) and 304L stainless steel (40 cm×30 cm) substrates, respectively. Before deposition, all the substrates were ultrasonically cleaned in acetone and ethanol. Then, they were rinsed by deionized water to ensure satisfactory surface roughness and cleanness. All the samples were prepared by a CAIP system (Fig.2), which was equipped with one Cr (99.99%) target and one $Al_{70}Cr_{30}$ (99.99%) target on the opposite sides of the chamber. The substrates were mounted on the base support with the help of sample holder. The base support was rotated at 5 rpm by using a DC motor to ensure surface uniformity in the deposition process. Prior to deposition, the chamber was pumped down to a base pressure below 5×10^{-3} Pa and the substrates were heated up to 200 ℃. Subsequently, the substrates were cleaned in situ by argon ion bombardment for 10 min with a negative bias voltage of 800 V at a pure argon pressure of 2.0 Pa. During the deposition of all Cr thin films, a target current of 65 A was applied to the Cr target and a negative voltage of 100 V to the substrates. All the depositions were performed at a fixed substrate to a target distance of 18 cm. The deposition time varied from 10 to 90 min for Cr thin films deposition. In this work, the optimization of film thickness was aimed to achieve the maximum IR reflectance for minimum emittance values for their possible use in spectrally selective coating structures. The film thickness was methodically investigated to achieve the minimum emittance, keeping other parameters constant during deposition. Finally, the solar selective absorbing coating (SSAC) of AlCrO/AlCrNO (LMVF)/AlCrN (HMVF)/Cr was prepared, in which the optimized Cr film was used as the IR reflector. The thermal stability of the SSAC and Cr thin film was studied at 600 °C for 10 h in air and vacuum.

2.2 Coating characterization

The structural analysis of the films was performed by a grazing incidence X-ray diffraction (GIXRD, Empyrean) using Cu-Kα (λ=0.15406 nm) radiation, which was operated at 40 kV and 40 mA with a glazing incidence angle of 0.5°. The scanning angular two theta was ranged fom 20° to 80° at a scanning speed of 5°/min. The surface and cross-sectional morphologies of the coatings were characterized by a Field Emission Scanning Electron Microscope (FE-SEM, Zeiss Ultra Plus) system operated at 5 kV. The surface topographies were probed using an Atomic Force Microscope (AFM, Shimadzu SPM-9500J3) operated in the tapping mode with a measuring area of 5 μm×5 μm. The chemical bonding stated were analyzed by an X-ray Photoelectron Spectroscopy (XPS, ESCALAB 250Xi) with Al-Kα ($h\nu$=1486.6 eV) radiation source at 20 kV voltage and 15 mA current, which was calibrated by the carbon peak C 1s at 284.8 eV. The background was subtracted by the Smart method, and deconvolution of the spectra were conducted using a non-linear least-square fit with a Lorentzian/Gaussian shape (L/G Mix 30%). The electrical resistivity of the obtained coatings was measured by a standard four-point probe system.

Optical properties of all the films were measured at room temperature. The near-normal spectral reflectance ($R(\lambda)$) and transmittance (T) in the wavelength range of 0.3-2.5 μm were measured by a UV-VIS-NIR spectrophotometer (Shimadzu UV3600). While, the spectral reflectance ($R(\lambda)$) in the wavelength range of 2.5-25 μm was measured by a Fourier Transform Infrared Spectrometer (Tensor 27, Bruker). The optical constants (n and k) of Cr thin films were obtained by modeling the measured reflectance and transmittance spectra with a commercial optical simulation program (CODE)[23]. The solar absorptance (α) and thermal emittance (ε) were calculatd by

$$\alpha=\frac{\int_{0.3}^{2.5} I_{\mathrm{sol}}(\lambda)(1-R(\lambda))\mathrm{d}\lambda}{\int_{0.3}^{2.5} I_{\mathrm{sol}}(\lambda)\mathrm{d}\lambda} \tag{1}$$

$$\varepsilon=\frac{\int_{2.5}^{2.5} I_{\mathrm{b}}(\lambda)(1-R(\lambda))\mathrm{d}\lambda}{\int_{2.5}^{25} I_{\mathrm{b}}(\lambda)\mathrm{d}\lambda} \tag{2}$$

where, $I_{\mathrm{sol}}(\lambda)$ is the solar radiation power at AM1.5, $R(\lambda)$ is the spectral reflectance, and $I_{\mathrm{b}}(\lambda)$ is the spectral black body emissive power at a room temperature of 25 ℃.

3 Results and discussion

3.1 Structural analysis

XPS was carried out to analyze the chemical

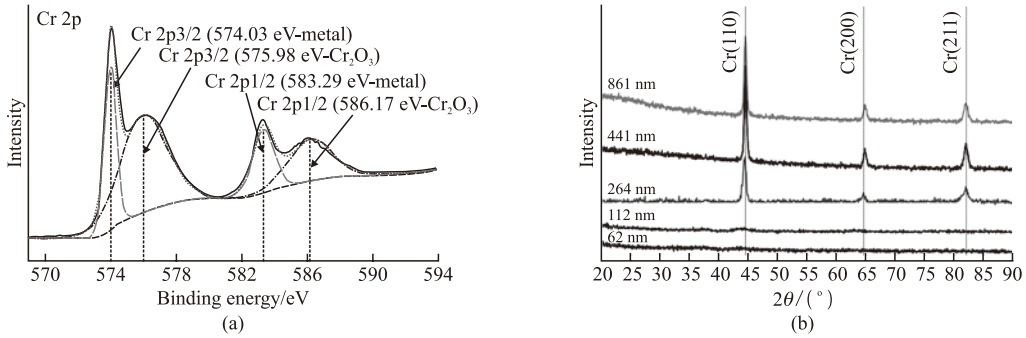

Fig.3 (a) The XPS core level spectrum from Cr 2p electrons of 441 nm thick deposited Cr thin film and (b) The XRD patterns of the Cr thin films prepared with varied thicknesses

structure of deposited Cr thin film. Fig.3(a) shows the XPS core level spectrum of Cr 2p electrons of Cr thin film with a thickness of 441 nm on stainless steel substrate, which showed two strong bands at around 575 eV and 585 eV corresponding to Cr 2p3/2 and Cr 2p1/2. These two bands could be decomposed into two pairs of peaks at 574.03 and 583.29 eV, 575.98 and 586.17 eV, which could be assigned to the metal Cr-Cr bond, oxide Cr-O bond, respectively. These peaks were compared with XPS database compiled by National Institute of Standard and Technology (NIST)[24]. The results also presented the oxygen content in the films that was probably due to the films exposure to the air ambient.

XRD studies were carried to analyze the evolution of Cr thin films structure and their correlation with absorptance and thermal emittance. The XRD patterns of Cr thin films on SS substrates with different thicknesses are shown in Fig.3(b). The XRD spectrum suggested that Cr thin films were polycrystalline with cubic crystallographic Cr phase (ICDD-PDF: 85-1335), but had preferred orientation along (110) plane. No other characteristic peaks related to impurities or other chromium oxide compounds were observed. These analyses confirmed that the element in the coating was pure chromium. Furthermore, the Cr thin films with smaller thickness (62-112 nm) were nearly amorphous and no significant diffraction of Cr diffraction pattern was observed. In the case of thicker films, only chromium diffraction peaks related to Cr (110), (200), and (211) were observed. Meanwhile, the crystallinity of the film was found to increase with increasing the thickness, due to the initial stress release for the deposited chromium thin films on SS substrates[25]. Because the structure evolution of Cr films was an atomistic process during the film deposition and affected by process parameters, such as deposition time. This may lead to the variation in grain size, texture orientation and film density of deposited thin film structures[26]. Due to the effects of crystallite size and lattice strain, the peak width increased, and the 2θ peak position shifted[27]. The lattice parameters of the Cr thin films deposited at various times are summarized in Table 1.

Table 1 The structure parameters of Cr thin films with different thicknesses

Thickness/nm	2θ/(°)	β_{hkl} /(°)	*hkl*	d_{hkl} /(nm)	Structure
62	-	-	-	-	Amorphous
112	-	-	-	-	Amorphous
	44.41	0.63	(110)	0.204	
264	64.50	0.72	(200)	0.144	Cubic
	81.80	0.68	(211)	0.118	
	44.47	0.46	(110)	0.204	
441	64.74	0.50	(200)	0.144	Cubic
	81.89	0.63	(211)	0.118	
	44.43	0.48	(110)	0.204	
861	64.92	0.66	(200)	0.144	Cubic
	81.83	0.68	(211)	0.118	

The crystallite size was usually calculated by Scherrer method, which deemed that the peak broadening occurred because of crystal sizes. However, lattice strain was a measure of the distribution of lattice dislocations affecting the peak broadening and position[28]. Thus, the lattice strain should be considered in crystallite size calculations. Several methods were designed for considering the lattice strain in crystallite size calculation. Among these methods, size strain plot (SSP) method was applied in the current research, which had the advantage that less weight was given to data from reflections at high angles, where the precision was usually lower[27]. In SSP, Lorentzian and Gaussian functions were employed to describe crystallite size and lattice strain, respectively. Accordingly, it could be written as[29]:

$$(d_{hkl}\beta_{hkl}\cos\theta)^2 = \frac{3}{4D}(d_{hkl}^2\beta_{hkl}\cos\theta) + (\frac{\varepsilon_0}{2})^2 \quad (3)$$

where, D is the crystallite size, and ε_0 is the lattice strain of Cr thin films. Theterm $(d_{hkl}\beta_{hkl}\cos\theta)^2$ was plotted with respet to $(d_{hkl}^2\beta_{hkl}\cos\theta)$ for all the orientation peaks of Cr thin films. The crystallite size and lattice strain could be calculated from sloop and y-intercept of the fitted data, respectively (Fig.4), which is presented in Table 2.

Table 2 Geometric parameters of Cr thin films with different thicknesses

Thickness/nm	D/nm	$\varepsilon_0/\times10^{-4}$
264	17.79	7.17
441	18.29	4.81
861	18.38	4.62

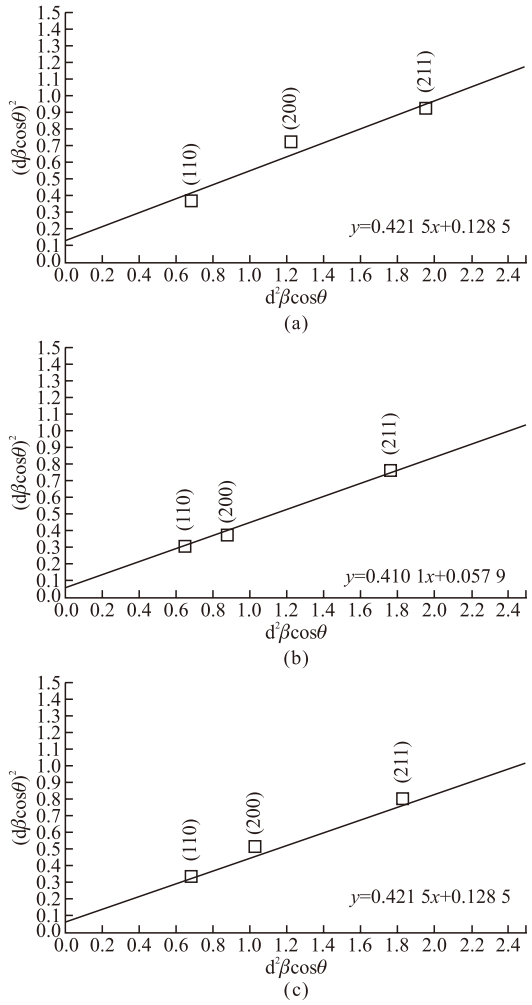

Fig.4 The SSP plot of the Cr thin films with thicknesses of (a) 264 nm, (b) 441 nm and (c) 861 nm

As the film thickness increased, the (110) diffraction peaks shifted to higher angles and the FWHM reduced, which indicated that grain growth had occurred. It was observed that the crystallite size increased with increasing film thickness. According to Daniel *et al*[30], most defects could be assumed located at and in grain boundaries. Thus, the relation of the volume fraction of grain boundaries to grains had a major influence on the strain. The thinner the films were, the smaller were the grains and the higher was the volume fraction of grain boundaries in between. Thus, the reduced grain boundary fraction in thicker films led to a reduced defect density and, hence, reduced the strain. The schematic development of Cr thin film structure could be summarized in Fig.5, as a function of thickness. The lower thickness of Cr film, up to 264 nm or less, led to highly disordered phase. As thickness increased with deposition time, the initial Cr layer acted as a buffer layer for upper Cr thin film structure. Thus, the crystallinity increased and the strain reduced, as observed in XRD measurement and summarized in Table 2. Finally, the pure Cr crystallographic phase was deposited, the crystallite size and strain kept almost unchanged at the film thickness of 441 nm.

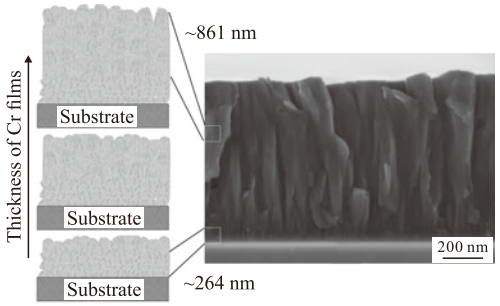

Fig.5 The schematic representation of Cr thin films with varying the thickness

3.2 Microstructure analysis

The 2D surface AFM imaged of Cr films are shown in Fig.6 for SS substrates deposited with different thicknesses. The granular morphology was observed for all Cr thin films, which showed an increase in granules size with increasing thickness, which was consistent with the XRD measurements. The root mean square surface roughness (R_{rms}) rose with increasing the deposition time. Initially, a decrease could be found for smaller film thickness, suggesting that surface defects had decreased, contributing towards reduced surface roughness. Then, the crystallite size increased with thickness, resulting in an increase in R_{rms} for thicker films.

The surface morphology of Cr thin films on SS substrates with different thicknesses is shown in Fig.6, in conjunction with AFM microstructure. The microstructure was uniform and dense throughout the film surface with granular morphology. It was clear that the size and shape of Cr grains significantly increased with film thickness. As the emittance was also a surface property of the materials, the low surface roughness

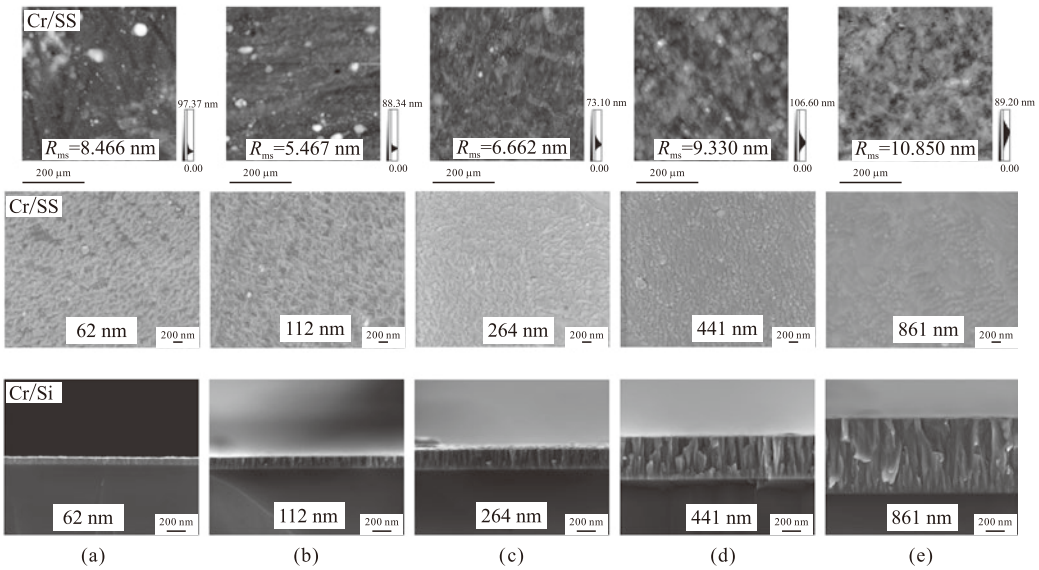

Fig.6 2D AFM images, FESEM surface and cross-sectional micrographs of Cr thin films with thicknesses of (a) 62 nm, (b) 112 nm, (c) 264 nm, (d) 441 nm and (e) 861 nm

of the film was important to achieve the low thermal emittance of the film.

The cross-sectional FESEM images of Cr thin films deposited on silicon substrates are depicted in Fig.6, indicating columnar microstructure, typical of films prepared by CAIP. A more careful inspection revealed the highly disordered phase of Cr films with smaller thickness, which also could be observed in the thicker films close to the silicon substrate.

3.3 Optical properties

3.3.1 Visible range

Fig.7 shows the reflectance spectra of the Cr thin films with increasing thickness. It was observed that the reflectance increased gradually from the film thickness 62 nm to 112 nm, and then reached the maximum in the thickness range of 441-861 nm. The variation of absorptance with the Cr thickness is shown in the inset of Fig.7, which was calculated by Eq.(1) and found to drop gradually. The variations of the reflectance spectra and absorptance of the Cr films attributed to its film growing process. The Cr film initially consisted of tiny crystals with hill-like rounded top and then grew to a dense smooth surface for the broadening of the hill-like tops with increasing film thickness (62-112 nm). As the film thickness increased from 264 nm to 441 nm, the crystallite size increased and the metal particles coalesced to form irregular length and shape, which could be found in Fig.6. When the metallic film reached a certain equivalent thickness, the dense and smooth surface of the Cr film kept unchanged with the continually increasing thickness from 441 nm to 861 nm, of which the reflectance spectra were nearly the same and reached the maximum.

The optical constants (n and k) of the Cr thin films as a function of thickness on quartz substrates are shown in Fig.8. The refractive index n and extinction coefficient k decreased with the film thickness increasing. The variation correlated with the film growth, which could be explained by the Bruggman's effective-medium approximation (BEMA)[18]. The crystallite size and some residual voids significantly altered the effective optical constants. During the initial deposition stage, the hill-like top Cr formed highly disordered phase on the substrates, and the area fraction occupied by the metal particles was small with many voids. With further deposition, the area fraction rose rapidly and the optical constants decreased. Then, the hill-like tops were linked and formed continuous film with less voids, where no major change was found in the microstructure, so the refractive index n and extinction k coefficient tended to be a constant level.

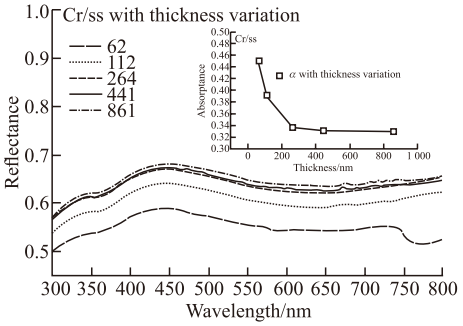

Fig.7 The reflectance curves in the visible range of Cr thin films with different thicknesses

3.3.2 Infrared range

The reflectance spectra were recorded for these Cr thin films in the 2.5-25 μm wavelength range, at

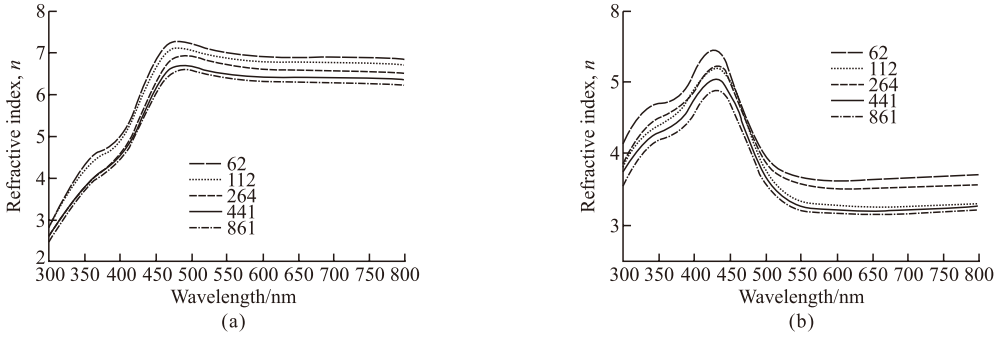

Fig.8 The refractive index n (a) and extinction coefficient k (b) of Cr thin films with different thicknesses on quartz substrates

room temperature of 25 ℃. The measured reflectance spectra are plotted in Fig.9, and used for calculating the thermal emittance according to Eq.(2). The calculated emittance values are plotted as an inset, as a function of deposition thickness in Fig.9. It could be observed that the emittance values strongly depended on the thickness of thin film structure, which showed a minimum emittance value of 0.0471 for the 60-90 min deposited Cr thin film with a thickness of 441-861 nm. Meanwhile, the emittance value became almost constant after certain thickness (441 nm), above which the emittance were nearly insensitive to the thickness. The decrease in emittance with thickness could be explained by the enhanced crystallinity and reduced defects, as observed from XRD, SEM, and AFM measurements. In another word, the low emittance for Cr thin films with large thickness were attributed to the reduced defects such as grain boundaries, dislocation, vacancies and interferential defects[2]. The free electrons in the metal thin films played an important role to minimize the thermal emittance, for the infrared property was determined by the contribution of free electrons in films[31].

Measurements of electrical resistivity of the deposited Cr thin films were carried out using the four-point probe method. For this, single Cr films were deposited on optical quartz to avoid the contribution of the substrate on the electrical measurements. Fig.10 shows the variation of electrical resistivities as a function of film thickness. The total normal emittance of metal film could be calculated using Hagen-Rubens relation and given by[31]:

$$\varepsilon=9.98\times10^{-3}\times R^{1/2}-5.30\times10^{-5}\times R+3.00\times10^{-7}\times R^{3/2} \quad (4)$$

where, R is the electrical resistivity in (μΩ•cm) at room temperature of 25 ℃. In thin films, the resistivity strongly depended on the crystallite size, thus, on the film thickness. This could be attributed to the lower overall defect densities in thicker films as already explained. The resistivity was higher for thinner films and reached a quite constant level for films above 264 nm thickness. The experimental emittance of the films were lower than the theoretical curve's, which trend was accordant. The experimental observations suggested that the minimum emittance values were achieved for Cr thin films deposited with a thickness above 441 nm. This optimized thickness could be used for preparing the Cr metallic infrared reflector thin films in conjunction with an absorber and antireflecting structure for the application of solar spectrally selective coating.

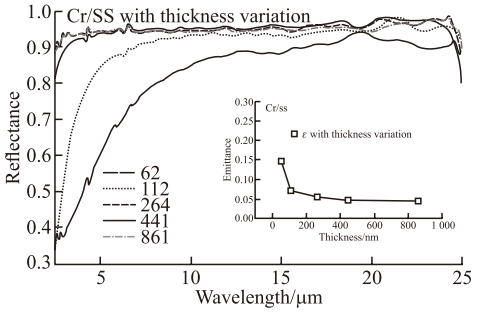

Fig.9 The reflectance curves in the infrared range of Cr thin films with different thicknesses

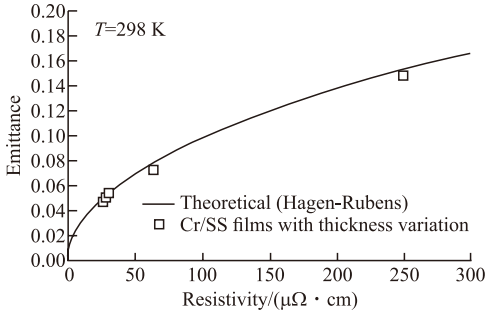

Fig.10 Total normal emittance of experimental Cr thin films as a function of resistivity

3.4 Performance of spectrally selective coating on Cr reflector

In order to study the effect of Cr interlayer on the emittance of spectrally selective coating on SS substrate, a tandem absorber consisting of a multilayer stack of AlCrO/AlCrNO (LMVF)/AlCrN (HMVF) was

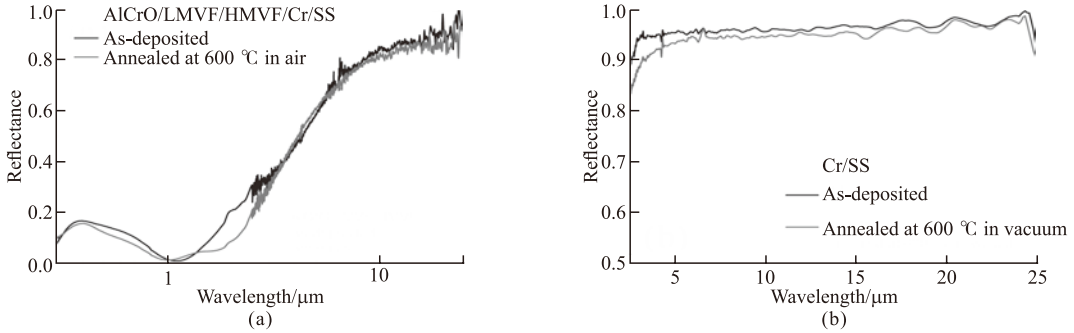

Fig.11 The reflectance spectra of the (a) SSAC and (b) Cr thin films before and after annealling

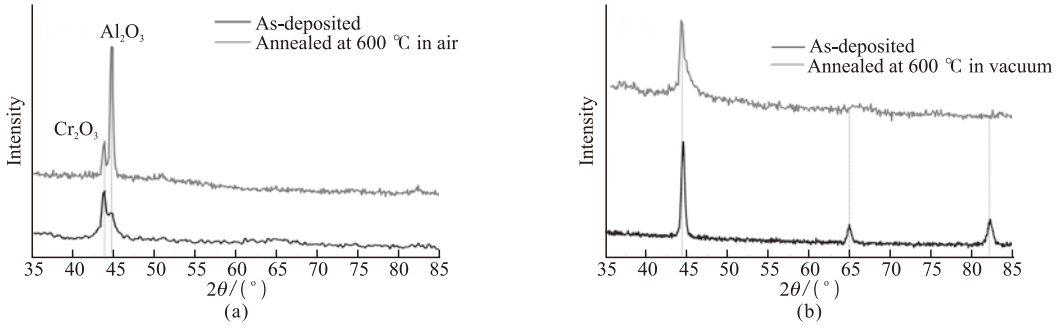

Fig.12 XRD patterns of (a) SSAC and (b) Cr thin films before and after annealing

deposited under optimized conditions with a Cr layer thickness of 461 nm, the details of which are provided elsewhere[16]. This coating exhibited an absorptance of 0.91 and emittance of 0.15. The corresponding reflectance spectra in the range of 0.3-25 μm is shown in Fig.11, depicting very high reflectance in the IR region. The Cr film, acting as an IR reflector, caused this high reflectance of the solar selective absorbing coating. The Cr thin film also improved the thermal stability of the SSAC by acting as a diffusion barrier between the SS substrate and tandem absorber.

Table 3 The solar absorptance and thermal emittance of samples before and after annealing

Sample	As-deposited		After-annealed		
	α	ε		α	ε
Cr/SS	0.33	0.05	Vacuum	0.34	0.06
AlCrO/AlCrNO/AlCrN/Cr/SS	0.91	0.14	Air	0.93	0.14

To demonstrate the high thermal stability of the solar selective absorbing coating, the as-deposited coating was heated at 600 ℃ for 10 h in air with a heating rate of 5 ℃/min. The Cr thin film were prepared between the substrate and spectrally selective coating. In order to simulate the thermal condition, the Cr thin film with a thickness of 461 nm was annealed at 600 ℃ for 10 h in vacuum with a heating rate of 5 ℃/min. The absorptance and thermal emittance of as-deposited and after-annealed samples are listed in Table 3. The absorptance of the SSAC increased from 0.91 to 0.93, while the thermal emittance almost kept unchanged at 0.06. Owing to the high IR reflectance of the Cr/SS IR reflector, the low thermal emittance of the SSAC was obtained.

To access the phase evolution of the coatings before and after heat treatment, the GIXRD analysis was performed in this investigation as shown in Fig.12. As for the SSAC shown in Fig.12(a), the coating was indicated to consist of Al_2O_3 and Cr_2O_3 before and after heat treatment, Moreover, the content of Al_2O_3 was remarkably increased after annealing. The XRD pattern of Cr thin film shown in Fig.12(b) shows a weakened plane of (110) due to the interdendritic diffusion and the diffusion of the substrate elements after annealing. It was assumed that the oxides formation on the spectrally selective coating surface increased the absorptance after annealing. While, the thermal emittance of the SSAC kept almost unchanged for the high reflectance of Cr thin film even after heat treatment. The Cr layer was expected to minimize the outward diffusion of SS substrate, and the structural stability and oxidation resistance of AlCrO, AlCrNO, and AlCrN layers were responsible for the overall thermal stability of the SSAC deposited on Cr coated substrate. Therefore, the optimized Cr thin film performed an excellent property of high reflectance as an IR reflector in SSAC.

4 Conclusions

CAIP deposited Cr thin films were studied and prepared, and the thickness was optimized in order to

achieve the minimum thermal emittance/maximum infrared reflectance in 2.5-25 μm wavelength range. The structure-thickness correlations suggested that the thermal emittance of Cr reflector strongly depended on film thickness. The minimum thermal emittance was obtained for Cr thin film structures with minimum dislocation densities and strain, and maximum crystallite sizes. The optimized film thickness above 441 nm showed the minimum thermal emittance of 0.05. The small variation in emittance values was attributed to the free electrons due to varied crystallite sizes. The highly reflective Cr layer caused low emittance of AlCrO/AlCrNO/AlCrN/Cr/SS coating. The coating deposited with optimal thickness Cr layer exhibited a relatively good thermal stability with a solar selectivity of 0.93/0.14 after annealing at 600 ℃ in air. The relative good thermal stability was due to the dense structure of AlCrO, AlCrNO, and AlCrN layers. The slightly higher emittance of the SSAC after annealing resulted from the oxides formed on the surface of AlCrO layer. The results suggested that the Cr metallic thin film with optimal thickness could be used as an effective infrared reflector for the development of SSAC structure.

References

[1] Usmani B, Vijay V, Chhibber C, *et al*. Optimization of Sputtered Zirconium Thin Films as an Infrared Reflector for Use in Spectrally-selective Solar Absorbers[J]. *Thin Solid Films*, 2017,627: 17-25

[2] Sibin KP, John S, Barshilia HC. Control of Thermal Emittance of Stainless Steel Using Sputtered Tungsten Thin Films for Solar Thermal Power Applications[J]. Sol. Energy Mater. Sol. Cells, 2015, 133: 1-7

[3] Lopez A, Roberts B, Heimiller D, *et al*. U.S. Renewable Energy Technical Potentials: a GISBased Analysis[R]. *National Renewable Energy laboratory, Golden*, CO, 2012

[4] Sampathkumar K, Arjunan TV, Pitchandi P, *et al*. Active Solar Distillation-a Detailed Review[J]. *Renewable Sustainable Energy Rev*., 2010, 14(6): 1 503-1 526

[5] Chen B, Zhuang Z, Chen X, *et al*. Field Survey on Indoor Thermal Environment of Rural Residences with Coupled Chinese Kang and Passive Solar Collecting Wall Heating in Northeast China[J]. *Sol. Energy*, 2007, 81(6): 781-790

[6] Feng JX, Zhang S, Lu Y, *et al*. The Spectral Selective Absorbing Characteristics and Thermal Stability of SS/TiAlN/TiAlSiN/Si_3N_4 Tandem Absorber Prepared by Magnetron Sputtering[J]. *Sol. Energy*, 2015, 111: 350-356

[7] Rebouta L, Capela P, Andritschky M, *et al*. Characterization of TiAlSiN/TiAlSiON/SiO_2 Optical Stack Designed by Modelling Calculations for Solar Selective Applications[J]. *Sol. Energy Mater. Sol. Cells*, 2012, 105: 202-207

[8] Gelin K, Boström T, Wäckelgård E. Thermal Emittance of Sputter Deposited Infrared Reflectors in Spectrally Selective Tandem Solar Absorbers[J]. *Sol. Energy*, 2004, 77(1): 115-119

[9] Feng JX, Zhang S, Liu X, *et al*. Solar Selective Absorbing Coatings TiN/TiSiN/SiN Prepared on Stainless Steel Substrates[J]. *Vacuum*, 2015, 121: 135-141

[10] Barshilia HC, Kumar P, Rajam KS, *et al*. Structure and Optical Properties of Ag-Al_2O_3 Nanocermet Solar Selective Coatings Prepared Using Unbalanced Magnetron Sputtering[J]. *Sol. Energy Mater. Sol. Cells*, 2011, 95(7): 1 707-1 715

[11] Nuru ZY, Arendse CJ, Nemutudi R, *et al*. Pt-Al_2O_3 Nanocoatings for High Temperature Concentrated Solar Thermal Power Applications[J]. *Phys. B* (Amsterdam, Neth.), 2012, 407(10): 1 634-1 637

[12] Zheng LQ, Zhou FY, Zhou ZD, *et al*. Angular Solar Absorptance and Thermal Stability of Mo–SiO_2 Double Cermet Solar Selective Absorber Coating[J]. *Sol. Energy*, 2015, 115: 341-346

[13] Valleti K, Krishna DM, Joshi SV. Functional Multi-layer Nitride Coatings for High Temperature Solar Selective Applications[J]. *Sol. Energy Mater. Sol. Cells*, 2014, 121: 14-21

[14] Liu HD, Fu TR, Duan MH, *et al*. Structure and Thermal Stability of Spectrally Selective Absorber Based on AlCrON Coating for Solar-thermal Conversion Applications[J]. *Sol. Energy Mater. Sol. Cells*, 2016, 157: 108-116

[15] Valleti K, Krishna DM, Reddy PM, *et al*. High Temperature Stable Solar Selective Coatings by Cathodic Arc PVD for Heat Collecting Elements[J]. *Sol. Energy Mater. Sol. Cells*, 2016, 145: 447-453

[16] Wang XB, Zhang XM, Li QY, *et al*. Spectral Properties of AlCrNO-based Multi-layer Solar Selective Absorbing Coating during the Initial Stage of Thermal Aging upon Exposure to Air[J]. *Sol. Energy Mater. Sol. Cells*, 2018, 185: 81-92

[17] Liu HD, Wan Q, Lin BZ, *et al*. The Spectral Properties and Thermal Stability of CrAlO-based Solar Selective Absorbing Nanocomposite Coating[J]. *Sol. Energy Mater. Sol. Cells*, 2014, 122: 226-232

[18] Sun XL, Hong RJ, Hou HH, *et al*. Thickness Dependence of Structure and Optical Properties of Silver Films Deposited by Magnetron Sputtering[J]. *Thin Solid Films*, 2007, 515(17): 6 292-6 966

[19] Selvakumar N, Barshilia HC. Review of Physical Vapor Deposited (PVD) Spectrally Selective Coatings for Mid- and High-temperature Solar Thermal Applications[J]. *Sol. Energy Mater. Sol. Cells*, 2012, 98: 1-23

[20] Zhao YH, Xu L, Guo CQ, *et al*. Effect of Axial Magnetic Field on the Microstructure and Mechanical Properties of CrN Films Deposited by Arc Ion Plating[J]. *Acta Metall. Sin*. (*Engl. Lett*.), 2017, 30 (7): 688-696

[21] Fan QX, Wang TG, Liu YM, *et al*. Microstructure and Corrosion Resistance of the AlTiN Coating Deposited by Arc Ion Plating[J]. *Acta Metall. Sin*. (Engl. Lett.), 2016, 29(12): 1 119-1 126

[22] Fan QX, Zhang JJ, Wu ZH, *et al*. Influence of Al Content on the Microstructure and Properties of the CrAlN Coatings Deposited by Arc Ion Plating[J]. *Acta Metall. Sin*. (*Engl. Lett*.), 2017, 30(12): 1 221-1 230

[23] Theiss M. Scout Thin Film Analysis Software Handbook[M]. *Hard And Software For Optical Spectroscopy, Aachen, Germany*, 2012

[24] *NIST X-ray Photoelectron Spectroscopy Database*. NIST Standard Reference Database 20, Version 4.1 [EB/OL]. 2012

[25] Zhu BL, Zhu SJ, Wang J, *et al*. Thickness Effect on Structure and Properties of ZAO Thin Films by RF Magnetron Sputtering at Different Substrate Temperatures[J]. *Phys. E Low-Dimensional Syst. Nanostructures*, 2011, 43: 1 738-1 745

[26] Sun H, Zhu X, Yang D, *et al*. Morphological and Structural Evolution during Thermally Physical Vapor Phase Growth of PbI2 Polycrystalline Thin Films[J]. *J. Cryst. Growth*, 2014, 405: 29-34

[27] Zak AK, Majid WHA, Abrishami ME, *et al*. X-ray Analysis of ZnO Nanoparticles by Williamson-Hall and Size-strain Plot Methods[J]. *Solid State Sci*., 2011, 13(1): 251-256

[28] Mote V, Purushotham Y, Dole B. Williamson-Hall Analysis in Estimation of Lattice Strain in Nanometer-sized ZnO Particles[J]. *J. Theor. Appl. Phys*., 2012, 6: 1-8

[29] Tagliente MA, Massaro M. Strain-driven (002) Preferred Orientation of ZnO Nanoparticles in Ion-implanted Silica[J]. *Nucl. Instrum Methods Phys. Res. B*., 2008, 266(7): 1 055-1 061

[30] Daniel R, Hole D, Bartosik M, *et al*. Size Effect of Thermal Expansion and Thermal/Intrinsic Stresses in Nanostructured Thin Films: Experiment and Model[J]. *Acta Mater*., 2011, 59(17): 6 631-6 645

[31] Modest MF. *Radiative Heat Transfer*[M]. 3rd ed. Academic Press, New York, 2012